217

YES

NATIONAL AERONAUTICS AND SPACE ADMINISTRATION

**MSC INTERNAL NOTE NO. 68-FM-130**

**June 5, 1968**

# FACTORS INFLUENCING THE GUIDANCE ACCURACY OF A PLANETARY PROBE


By Thomas B. Murtagh,
Advanced Mission Design Branch




MISSION PLANNING AND ANALYSIS DIVISION

MANNED SPACECRAFT CENTER
HOUSTON, TEXAS

MSC INTERNAL NOTE NO. 68-FM-130

# FACTORS INFLUENCING THE GUIDANCE ACCURACY OF A PLANETARY PROBE

By Thomas B. Murtagh
Advanced Mission Design Branch

June 5, 1968

MISSION PLANNING AND ANALYSIS DIVISION
NATIONAL AERONAUTICS AND SPACE ADMINISTRATION
MANNED SPACECRAFT CENTER
HOUSTON, TEXAS

Approved: Jack Funk
Jack Funk, Chief
Advanced Mission Design Branch

Approved: J P Mayer
John P. Mayer, Chief
Mission Planning and Analysis Division

PRECEDING PAGE BLANK NOT FILMED.

CONTENTS

## FIGURES

| Figure | | Page |
|---|---|---|
| | (c) Entry speed . . . . . . . . . . . . . . . . . . . . | 33 |
| 8 | Spacecraft errors | |
| | (a) Navigation . . . . . . . . . . . . . . . . . . . . | 34 |
| | (b) Guidance . . . . . . . . . . . . . . . . . . . . | 35 |

FACTORS INFLUENCING THE GUIDANCE ACCURACY

OF A PLANETARY PROBE

By Thomas B. Murtagh


## SUMMARY

The influence of the type (i.e., relative range, range rate, or both) and accuracy of spacecraft onboard radar data, nominal entry parameters for the probe trajectory, and planet radius uncertainty for unmanned planetary probe guidance is presented. The probe is assumed to be deployed from a manned spacecraft at the destination planet's sphere of influence, with the inclination of the probe trajectory equal to that of the spacecraft approach hyperbola. The results of the analysis indicate that a probe entry guidance corridor of the order of 20 n. mi. can be obtained for a total midcourse $\Delta V$ less than 100 fps, with spacecraft onboard radar range data contributing more information to entry corridor determination than range-rate data. These results were more sensitive to nominal entry trajectory parameter variations than to variations in the assumed error in the radius of the target planet.


## INTRODUCTION

The analysis presented in this note extends and investigates some of the assumptions of reference 1 in more detail. The most significant assumption was that the radar onboard the manned spacecraft could measure precisely the type of data - relative range and/or range-rate - to the unmanned probe. That is, the onboard estimates of the state vectors for the probe and spacecraft have equivalent accuracy. The nominal probe entry trajectory was also specified so that the probe would arrive at the nominal entry altitude approximately one hour before the spacecraft arrived at periapsis of the approach hyperbola. These nominal entry parameters were fixed in order to simplify the analysis. However, the entry parameters are a function of the type of probe mission considered. For example, shallow entry flight-path angles would be desired for probe missions which require a "skip-out" of the atmosphere into an orbit about the planet; impact-type probes require much steeper flight-path angles. For the analysis presented, a reference probe mission was chosen for determining the effect of the type and accuracy of spacecraft onboard

radar data on the guidance corridor. Variations in planet radius error and nominal entry trajectory parameters are presented in order to illustrate their effect on the entry corridor.

The results are presented for a conjunction class Mars mission and can be considered valid for other missions with similar characteristics.

## SYMBOLS

| | |
|---|---|
| $A(t)$ | sensitivity vector which relates star/planet-horizon included angle deviations to spacecraft state vector deviations |
| $B(t)$ | sensitivity matrix which relates spacecraft to probe relative range and range-rate deviations to spacecraft to probe state vector deviations |
| $C(t)$ | $6 \times 3$ compatability matrix defined by $\begin{pmatrix} 0 \\ I \end{pmatrix}$ |
| $E_p(t)$ | probe uncertainty covariance matrix |
| $E_s(t)$ | spacecraft uncertainty covariance matrix |
| $G(t)$ | $6 \times 6$ guidance matrix |
| $G_1(t)$, $G_2(t)$ | $3 \times 3$ sub-matrices of the guidance matrix |
| $H(t)$ | $3 \times 12$ sensitivity matrix defined by equation (9) |
| $I$ | identity matrix of appropriate dimensions |
| $K(t)$ | weighting matrix defined in equation (13) |
| $L(t)$ | $3 \times 3$ matrix defined by equation (16) |
| $M(t)$ | $3 \times 3$ matrix defined in equation (13) |
| $N(t)$ | covariance matrix of velocity correction execution error |
| $P(t)$ | $12 \times 12$ uncertainty covariance matrix for coupled spacecraft/probe system |

| | |
|---|---|
| $R(t)$ | covariance matrix of measurement errors defined by equation (14) |
| $r_B$ | planet radius |
| $\vec{r}_p$ | probe position vector with respect to planet |
| $\vec{r}_s$ | spacecraft position vector with respect to planet |
| $r_s$ | magnitude of spacecraft position vector |
| $\hat{r}_{star}$ | unit vector to a star |
| $t$ | current time |
| $\vec{V}_p$ | velocity vector of probe with respect to planet |
| $\vec{V}_s$ | velocity vector of spacecraft with respect to planet |
| $\vec{V}_\rho$ | spacecraft/probe relative velocity vector ($= \vec{V}_p - \vec{V}_s$) |
| $X_p(t)$ | probe dispersion covariance matrix |
| $X_s(t)$ | spacecraft dispersion covariance matrix |
| $\beta(t)$ | star/planet-horizon included angle |
| $\Gamma(\tau,t)$ | $6 \times 6$ probe state transition matrix |
| $\delta(\ )$ | small deviation from reference value of ( ) |
| $\Delta E(t)$ | degradation to $E_p(t)$ as result of spacecraft/probe separation maneuver |
| $\zeta(t)$ | 12-dimensional augmented state vector |
| $\theta(t)$ | one-half planet disc subtended angle ($\sin \theta = r_B/r_s$) |
| $\Theta(\tau,t)$ | $12 \times 12$ augmented state transition matrix defined by equation (3) |

| | |
|---|---|
| $\vec{\rho}(t)$ | relative position vector of probe with respect to spacecraft ($\vec{\rho} = \vec{r}_p - \vec{r}_s$) |
| $\rho(t)$ | magnitude of relative position vector |
| $\dot{\rho}(t)$ | spacecraft/probe relative range-rate ($= \frac{\vec{\rho}}{\rho} \cdot \vec{V}_\rho$) |
| $\sigma_\beta^{\ 2}$ | variance of star/planet-horizon observable |
| $\sigma_\rho^{\ 2}$ | onboard radar range variance |
| $\sigma_{\dot{\rho}}^{\ 2}$ | onboard radar range-rate variance |
| $\tau$ | projected time |
| $\Phi(\tau,t)$ | $6 \times 6$ spacecraft state transition matrix |

Supercripts:

| | |
|---|---|
| $(\ )^+$ | ( ) after navigation measurement or guidance maneuver |
| $(\ )^-$ | ( ) before navigation measurement or guidance maneuver |
| $(\ )^{-1}$ | Inverse of ( ) |
| $(\ )^T$ | Transpose of ( ) |

## ANALYSIS

### Assumptions

Following are the postulates for this analysis:

1. The unmanned probe is deployed from the manned spacecraft at the destination planet sphere of influence (SOI) so that the inclination of the probe trajectory equals that of the spacecraft approach hyperbola.

2. Spacecraft and probe position and velocity uncertainties are reduced by simultaneously processing onboard radar relative range and/or range-rate data and star/planet-horizon included angle data from the spacecraft using a Kalman filter.

3. Conic reference trajectories were assumed, and the state transition matrix used to propagate the errors was derived analytically for two-body conic trajectories.

4. Variable time of arrival (VTA) guidance logic was used to compute the root-mean-square (RMS) velocity corrections for the probe and the corresponding vacuum periapsis radius dispersions. The probe entry guidance corridor is computed by multiplying the radius dispersion by a factor of six ($\pm 3\sigma$ about the nominal).

5. A summary of the navigation and guidance system nominal errors is presented in table I. The spacecraft onboard radar errors are consistent with the values used in reference 2.

## Reference Mission

The reference mission chosen for the analysis presented in this note was a 1977 Mars stopover (ref. 3) which has an outbound trip time of 360 days, a Mars orbit time of 300 days, and a return to Earth time of 320 days. The reference trajectory characteristics for this mission are summarized in table II.

The Earth-injection covariance matrix for this trajectory was diagonal with RMS position and velocity errors of 4 n. mi. and 16 fps. Earth-based radar range and range-rate data were processed during the departure phase of the mission, i.e., within the Earth SOI, and was followed by onboard sextant planet-star tracking in the heliocentric phase, i.e., between the Earth and Mars SOI's. For these onboard measurements the sighting body was selected according to the optimality criteria outlined in reference 4. The error model for the Earth-based radar system is discussed in reference 5; the onboard sextant error model can be found in reference 1.

The Earth-based radar and onboard optical navigation data were processed every 30 minutes and each half-day during the departure and heliocentric phases, respectively. Three midcourse fixed time of arrival (FTA) velocity corrections requiring a total $\Delta V$ of 74.12 fps were executed to update the spacecraft dispersion matrix prior to the unmanned probe deployment at the Mars SOI (approximately 312 000 n. mi. from the planet).

## Spacecraft/Probe Navigation and Guidance System

The spacecraft/probe tracking geometry is illustrated in figure 1. For the study presented in this note it was assumed that the spacecraft onboard radar could measure the relative range and/or range-rate to the

probe and simultaneously use an onboard optical sensor, i.e., sextant, to measure the included angle between the Mars horizon and a star. This procedure seems feasible since the onboard radar can track the probe continuously and, when the spacecraft horizon-star measurement is fed into the onboard computer, a command could automatically be set up in the navigation program which would call for simultaneous data processing of the radar range and/or range-rate information.

The navigation data can be processed in the onboard computer using a Kalman filter. The structure of the filter equations for the coupled spacecraft/probe system is identical to the conventional Kalman equations but has increased state vector dimensions (ref. 2 and 6). For the problem considered here, the state vector is 12-dimensional and includes the spacecraft position and velocity as well as the position and velocity of the unmanned probe. The equation which relates deviations in this state vector at time, $\tau$, to deviations at time, t, is

$$\begin{bmatrix} \delta\vec{r}_s(\tau) \\ \delta\vec{V}_s(\tau) \\ \delta\vec{r}_p(\tau) \\ \delta\vec{V}_p(\tau) \end{bmatrix} = \begin{bmatrix} \Phi(\tau,t) & 0 \\ 0 & \Gamma(\tau,t) \end{bmatrix} \begin{bmatrix} \delta\vec{r}_s(t) \\ \delta\vec{V}_s(t) \\ \delta\vec{r}_p(t) \\ \delta\vec{V}_p(t) \end{bmatrix} \tag{1}$$

where $\Phi(\tau,t)$ and $\Gamma(\tau,t)$ are the $6 \times 6$ spacecraft and probe state transition matrices respectively. If we define

$$\delta\vec{\zeta}(\tau) = \begin{bmatrix} \delta\vec{r}_s(\tau) \\ \delta\vec{V}_s(\tau) \\ \delta\vec{r}_p(\tau) \\ \delta\vec{V}_p(\tau) \end{bmatrix} \tag{2}$$

and

$$\Theta(\tau,t) = \begin{bmatrix} \Phi(\tau,t) & 0 \\ 0 & \Gamma(\tau,t) \end{bmatrix} \tag{3}$$

then equation (1) becomes

$$\delta\vec{\zeta}(\tau) = \Theta(\tau,t)\ \delta\vec{\zeta}(t) \tag{4}$$

The initial 12 × 12 covariance matrix for the coupled system, i.e., at spacecraft/probe separation, is defined by

$$P(t_o) = \begin{bmatrix} E_s\ (t_c) & 0 \\ 0 & E_p(t_o) \end{bmatrix} \tag{5}$$

where $E_s(t_o)$ is the spacecraft uncertainty covariance matrix and

$$E_p(t_o) = E_s(t_o) + \Delta E(t_o) \tag{6}$$

The term $\Delta E(t_o)$ is the degradation to the probe uncertainty matrix as a result of the assumed imperfect separation maneuver. The equation for propagating this matrix between measurements is given by the expression

$$P(\tau) = \Theta(\tau,t)P(t)\Theta^T(\tau,t) \tag{7}$$

The equation which relates deviations in the observables, i.e., star horizon included angle, range, and range-rate, to state vector deviations is

$$\begin{bmatrix} \delta\beta(\tau) \\ \delta\rho(\tau) \\ \delta\dot{\rho}(\tau) \end{bmatrix} = H(\tau)\delta\vec{\zeta}(\tau) \tag{8}$$

where the 3 × 12 matrix $H(\tau)$ is written in partitioned form as

$$H(\tau) = \begin{bmatrix} A(\tau) & 0 \\ -B(\tau) & B(\tau) \end{bmatrix} \tag{9}$$

The vector $A(\tau)$ is defined by

$$A(\tau) = \left[ \frac{\partial \beta}{\partial \vec{r}_s} \quad \frac{\partial \beta}{\partial \vec{V}_s} \right] \tag{10}$$

and the $2 \times 6$ matrix $B(\tau)$ is given by

$$B(\tau) = \begin{bmatrix} \dfrac{\partial \rho}{\partial \vec{\rho}} & \dfrac{\partial \rho}{\partial \vec{V}_\rho} \\ \\ \dfrac{\partial \dot{\rho}}{\partial \vec{\rho}} & \dfrac{\partial \dot{\rho}}{\partial \vec{V}_\rho} \end{bmatrix} \tag{11}$$

The partial derivatives required in equations (10) and (11) can be computed from the following relationships (fig. 1).

$$\left.\begin{aligned} \frac{\partial \beta}{\partial \vec{r}_s} &= \frac{r_B}{r_s{}^3 \cos\theta}\,\vec{r}_s + \frac{\vec{r}_s \times (\vec{r}_s \times \hat{r}_{star})}{r_s{}^2 \left|\vec{r}_s \times \hat{r}_{star}\right|} \\ \frac{\partial \beta}{\partial \vec{V}_s} &= 0 \end{aligned}\right\} \tag{12a}$$

$$\left.\begin{aligned} \frac{\partial \rho}{\partial \vec{\rho}} &= \frac{\vec{\rho}^{\,T}}{\rho} \\ \frac{\partial \rho}{\partial \vec{V}_\rho} &= 0 \end{aligned}\right\} \tag{12b}$$

$$\left.\begin{aligned}\frac{\partial\dot{\rho}}{\partial\vec{\rho}} &= \frac{\vec{V}_\rho^{\,T}}{\rho}\left[I - \frac{\vec{\rho}\vec{\rho}^{T}}{\rho^2}\right]\\ \frac{\partial\dot{\rho}}{\partial\vec{V}_\rho} &= \frac{\vec{\rho}^{T}}{\rho}\end{aligned}\right\}\qquad(12c)$$

The equations required to update the uncertainty matrix, $P(\tau)$, at the time of a measurement can now be written

$$\left.\begin{aligned}P^{+}(\tau) &= \Big[I - K(\tau)H(\tau)\Big]\;P^{-}(\tau)\\ K(\tau) &= P^{-}(\tau)H^{T}(\tau)M^{-1}(\tau)\\ M(\tau) &= H(\tau)P^{-}(\tau)H^{T}(\tau)+R(\tau)\end{aligned}\right\}\qquad(13)$$

where the $3 \times 3$ covariance matrix of measurement errors, $R(\tau)$, is defined by

$$R(\tau) = \begin{bmatrix}\sigma_\beta^{\;2} & 0 & 0\\ 0 & \sigma_\rho^{\;2} & 0\\ 0 & 0 & \sigma_{\dot{\rho}}^{\;2}\end{bmatrix}\qquad(14)$$

and the (-) and (+) superscripts refer to a quantity before and after the measurement (or correction) respectively.

If it is assumed that the navigation and guidance systems are uncoupled, then the spacecraft and probe dispersion matrices are propagated separately using the equations

$$\left.\begin{aligned}X_s(\tau) &= \Phi(\tau,t)X_s(t)\Phi^{T}(\tau,t)\\ X_p(\tau) &= \Gamma(\tau,t)X_p(t)\Gamma^{T}(\tau,t)\end{aligned}\right\}\qquad(15)$$

When reasonable confidence is obtained in the trajectory estimates of either the probe or spacecraft, guidance maneuvers are commanded for the appropriate vehicle to restore the dispersed trajectory to specified nominal conditions. For example, if a guidance correction is commanded for the probe at time, $\tau$, then the RMS estimate of the required $\Delta V$ is computed from the square root of the trace of the equation

$$L(\tau) = \left[G_1(\tau)\ G_2(\tau)\right] \left[X_p(\tau)-P_4(\tau)\right]\left[G_1(\tau)\ \ G_2(\tau)\right]^T \quad (16)$$

where $G_1(\tau)$ and $G_2(\tau)$ are submatrices of the guidance matrix $G(\tau)$ discussed in references 1 and 7. The matrix $P_4(\tau)$ is a submatrix of the augmented uncertainty matrix $P(\tau)$ defined by

$$P(\tau) = \begin{bmatrix} P_1(\tau) & P_2(\tau) \\ P_3(\tau) & P_4(\tau) \end{bmatrix} \quad (17)$$

after one or more navigation measurements are processed.

The probe uncertainty and dispersion matrices are modified according to the equations (ref. 1)

$$\left.\begin{aligned} P_4^{+}(\tau) &= P_4^{-}(\tau) + CN(\tau)C^T \\ X_p^{+}(\tau) &= \left[I+G(\tau)\right] \left[X_p^{-}(\tau)-P_4^{-}(\tau)\right] \left[I+G(\tau)\right]^T+P_4^{+}(\tau) \end{aligned}\right\} \quad (18)$$

Equations similar to (16) and (18) are used to calculate the RMS $\Delta V$ and matrix updates for the spacecraft if $X_p(\tau)$ and $P_4(\tau)$ are replaced by $X_s(\tau)$ and $P_1(\tau)$ respectively. The covariance matrix of velocity correction execution error, $N(\tau)$, is derived and discussed in reference 8.

## RESULTS

### Nominal Probe Trajectory

Assuming that the probe is deployed from the spacecraft at the Mars SOI so that the inclination of the probe trajectory equals that of the

spacecraft approach hyperbola, three entry parameters remain to be specified - altitude, speed, and flight-path angle. The entry altitude assumed for the probe nominal trajectory was 315 000 ft. Figure 2 presents plots of probe separation $\Delta V$ versus entry speed for entry flight-path angles of $0^\circ$ and $-45^\circ$ and for this entry altitude. The minimum separation velocity occurs when the angle between the separation $\Delta V$ vector and the spacecraft velocity vector is $90^\circ$. From figure 2(a) it can be seen that the effect of variations in entry flight-path angle becomes more pronounced as the minimum of the curve is approached and decreases quite rapidly on either side of the minimum. The time required for the probe to reach vacuum periapsis (not shown on the figure) is inversely proportional to the entry speed. For the nominal probe trajectory an entry speed of 18 350 fps was chosen, with an entry flight-path angle of $-5^\circ$. These values of entry parameters cause the probe to reach its vacuum periapsis approximately 20 minutes ahead of the spacecraft arrival at the periapsis of the approach hyperbola. The separation $\Delta V$ required was 45 fps.

The spacecraft/probe relative range is plotted against time from separation for the nominal probe trajectory in figure 3. This relative range as a function of time depends upon the separation $\Delta V$ which, in turn, is a function of the specified entry parameters. The nominal probe trajectory chosen is very dependent on the relative range since the spacecraft onboard radar must have a maximum range beyond which no tracking is possible. The maximum range to the probe for the above nominal trajectory was about 2800 n. mi. so that effective probe tracking could be assumed throughout the probe delivery phase of the mission, if the onboard radar range capability was at least that value.

## Influence of the Type of Onboard Radar Data

The effect of the type of spacecraft onboard radar data and accuracy on the unmanned probe navigation is illustrated in figure 4. In figure 4(a) it is assumed that the onboard radar processes both range and range-rate data every 30 minutes for three sets of range and range-rate errors. The profile of the curves in this figure is not entirely what one would expect. The apparent anomaly in the data occurs between 10 and 50 hours from separation. Within this time span the larger radar errors produce lower projected vacuum periapsis radius uncertainties than the corresponding smaller radar errors. The explanation for this phenomena is related to the correlation which exists in the uncertainty matrix for the coupled spacecraft/probe system. It should be pointed out that the data weights, i.e., K(t), computed by the filter are a function of both the spacecraft and the probe uncertainties propagated from a previous measurement. In the region 10 - 40 hours from separation, the $\sigma_\rho = 200$ ft and $\sigma_{\dot\rho} = 2$ fps radar errors produce lower projected probe uncertainties than $\sigma_\rho = 100$ ft and $\sigma_{\dot\rho} = 1$ fps radar errors. The spacecraft errors, however,

projected to the periapsis of the approach hyperbola (data not shown) during this same time interval are slightly larger for the higher radar errors, i.e., $\sigma_\rho = 200$ ft and $\sigma_{\dot\rho} = 2$ fps, compared to values for the $\sigma_\rho = 100$ ft and $\sigma_{\dot\rho} = 1$ fps radar errors. This implies that the filter, in this time interval, gave more weight to the probe data compared to the simultaneously processed spacecraft data. A similar effect occurs between 40 and 50 hours from separation for the $\sigma_\rho = 300$ ft and $\sigma_{\dot\rho} = 3$ fps radar errors. The explanation is equivalent to that presented above.

Figures 4(b), 4(c), and 4(d) present probe navigation data comparing the three possible radar data type combinations, again assuming that data was processed every 30 minutes. In these figures the range and range-rate curve was generated by simultaneously processing range and range-rate information in the filter. The range curve was calculated by processing only range data in the filter in a separate simulation run. A third computer run was required to generate the range-rate curve by processing only range-rate data in the filter described by equations (13).

In figure 4(b), between 28 and 57 hours from probe deployment, the range-only tracking provides a lower vacuum periapsis radius uncertainty than the combination of range and range-rate tracking. This effect is due to the low information content of the range-rate data which tends to degrade the range and range-rate combination. This effect is present to a lesser degree in figures 4(c) and 4(d). A possible explanation is that the relative weight of the range-rate data compared to the range data has diminished as the errors were increased.

The probe guidance plots associated with the navigation data in figure 4 are presented in figure 5. Figure 5(a) illustrates the effect of the radar errors on the probe entry guidance corridor when range and range-rate data are processed every 30 minutes. Assume for the moment that a vacuum periapsis radius dispersion of 4 n. mi. is desired (corridor = 24 n. mi.). The nominal radar errors achieve this specified dispersion for an RMS midcourse $\Delta V$ equal to 80 fps. Increasing the radar errors by a factor of two approximately doubles the $\Delta V$ required to achieve this same dispersion. Increasing the radar errors by a factor of three, however, does not triple the required $\Delta V$.

Figures 5(b), 5(c), and 5(d) illustrate the effect of the type of radar tracking on the guidance corridor for the three sets of radar errors. In these plots it is obvious that range-rate data alone will not allow the probe to achieve the specified 24-n. mi. guidance corridor. An examination of figure 3 verifies this result. In that figure it is evident that the rate-of-change of the relative range is constant between the time of probe deployment and 55 hours from separation, implying

an insensitivity of the range-rate measurement to probe state vector variations. And, in all the cases shown, the range-only tracking produces this corridor for less ΔV than the range and range-rate tracking combination.

## Influence of Mars Radius Uncertainty

The effect of the Mars radius error on the probe entry guidance corridor is illustrated in figure 6. Nominal radar errors are assumed, with range and range-rate measurements processed simultaneously every 30 minutes, using the nominal probe reference trajectory previously discussed. If a guidance corridor of 24 n. mi. is desired (vacuum periapsis radius dispersion = 4 n. mi.) then the midcourse ΔV required are 30, 60, and 100 fps for Mars radius errors of 2, 10, and 20 n. mi.

## Influence of Varying Nominal Probe Trajectory Parameters

The effect of nominal trajectory parameter variation on probe guidance accuracy using nominal Mars radius and spacecraft onboard radar errors is presented in figure 7. Navigation data was processed every 30 minutes.

In figure 7(a) the probe midcourse ΔV is plotted as a function of the RMS vacuum periapsis radius dispersion for three values of entry altitude. The other entry parameters were fixed at their nominal values. As the entry altitude increases, the separation ΔV increases and the time from separation to vacuum periapsis decreases. The midcourse ΔV, for a given vacuum periapsis radius error, also increases as the entry altitude increases. It should be pointed out that the maximum relative range between the spacecraft and probe also increases with increases in the entry altitude. Consequently these guidance results are valid only if the onboard radar range capability is equal to or greater than 7500 n. mi. Otherwise effective probe tracking cannot be assumed throughout its delivery to the entry interface.

Variations in the entry flight-path angle are considered in figure 7(b). As the flight-path angle decreases, the separation ΔV increases slightly and the time to the probe vacuum periapsis remains almost constant. For a specified corridor the midcourse ΔV decreases as the flight-path angle is varied from $-5^\circ$ to $-40^\circ$.

Finally, variations in entry speed are illustrated in figure 7(c). Decreasing the entry speed produces corresponding reductions in the midcourse ΔV necessary to achieve a specified corridor.

## Spacecraft Navigation and Guidance

All of the data discussed in the preceding sections involved the probe navigation and guidance. The spacecraft from which the probe is deployed must also be maneuvered to some safe target dispersion. However, in order to keep the dimensions of this note within reasonable limits only a brief sketch of spacecraft data will be presented (fig. 8).

Figure 8(a) presents the spacecraft navigation data from spacecraft/probe separation to the approximate time of spacecraft arrival at the periapsis of the approach hyperbola. Similar data was presented in reference 1. The solid curve represents the projected periapsis radius uncertainty assuming that no probe tracking occurs, with Mars-horizon/star included angle measurements processed every 30 minutes. The dashed curve presents analogous data assuming that the spacecraft now tracks the probe. It should be noted that better navigation results are obtained when the spacecraft tracks the probe than when it does not. This is a result of coupling the spacecraft/probe system through the measurements of relative range and range-rate. The effect noted here is quite analogous to reducing landmark location error in orbital navigation problems. There a spacecraft in orbit about a planet makes optical sightings to poorly defined landmarks and the output of the data processing system reduces the landmark position uncertainty as well as the uncertainty associated with the state of the orbiting spacecraft.

The spacecraft guidance results are presented in figure 8(b). Again an improvement is noted when the spacecraft tracks the probe as compared to the case when it does not. For example, if a $1\sigma$ periapsis radius dispersion of 3 n. mi. is specified, a midcourse $\Delta V$ of 13 fps is required if the spacecraft is tracking the probe compared to 25 fps if it is not tracking.

The lower values of spacecraft $\Delta V$ for a specified periapsis radius dispersion compared to the probe results presented in the previous sections is due to the fact that the initial spacecraft errors are smaller than the probe errors. [See equation (6).] If there were no probe deployment execution errors, i.e., $\Delta E(t_o) = 0$, then the spacecraft and probe guidance results would be approximately the same.

## CONCLUDING REMARKS

The influence of the type and accuracy of spacecraft onboard radar data, nominal entry trajectory parameters, and planet radius error for unmanned planetary probe guidance has been presented. The results of the study indicate that a probe guidance corridor of about 20 n. mi.

can be obtained for a total midcourse $\Delta V$ around 100 fps, and that the spacecraft onboard radar relative range data contribute more information to entry corridor determination that the relative range-rate data. For the cases run, the corridor results were more sensitive to nominal entry trajectory parameter variations than to variations in the assumed uncertainty in the planet radius.

TABLE I.- NOMINAL 1 σ RMS G&N ERRORS

(a) Navigation system

| | |
|---|---|
| Onboard radar | |
| Range, ft | 100 |
| Range rate, fps | 1 |
| Onboard sextant, arc sec | 10 |
| Mars radius, n. mi. | 10 |

(b) Guidance system

| | |
|---|---|
| Proportional percent | 1 |
| Pointing, deg | 1 |
| Cutoff, fps | 0.5 |

TABLE II.- CHARACTERISTICS OF THE 1977 MARS STOPOVER REFERENCE MISSION

| | |
|---|---|
| Launch from earth, Julian date . . . . . . . . . . . . . . . . | 2 443 440 |
| Earth injection velocity magnitude, fps . . . . . . . . . . | 12 652 |
| Outbound trip time, days . . . . . . . . . . . . . . . . . . . | 360 |
| Mars stopover time, days . . . . . . . . . . . . . . . . . . . | 300 |
| Return trip time, days . . . . . . . . . . . . . . . . . . . . | 320 |
| Periapsis altitude at Mars, n. mi.[a] . . . . . . . . . . . . | 200 |
| Entry velocity at earth, fps . . . . . . . . . . . . . . . . . | 38 463 |

[a]The Mars approach hyperbola periapsis is located in the Martian Southern hemisphere.

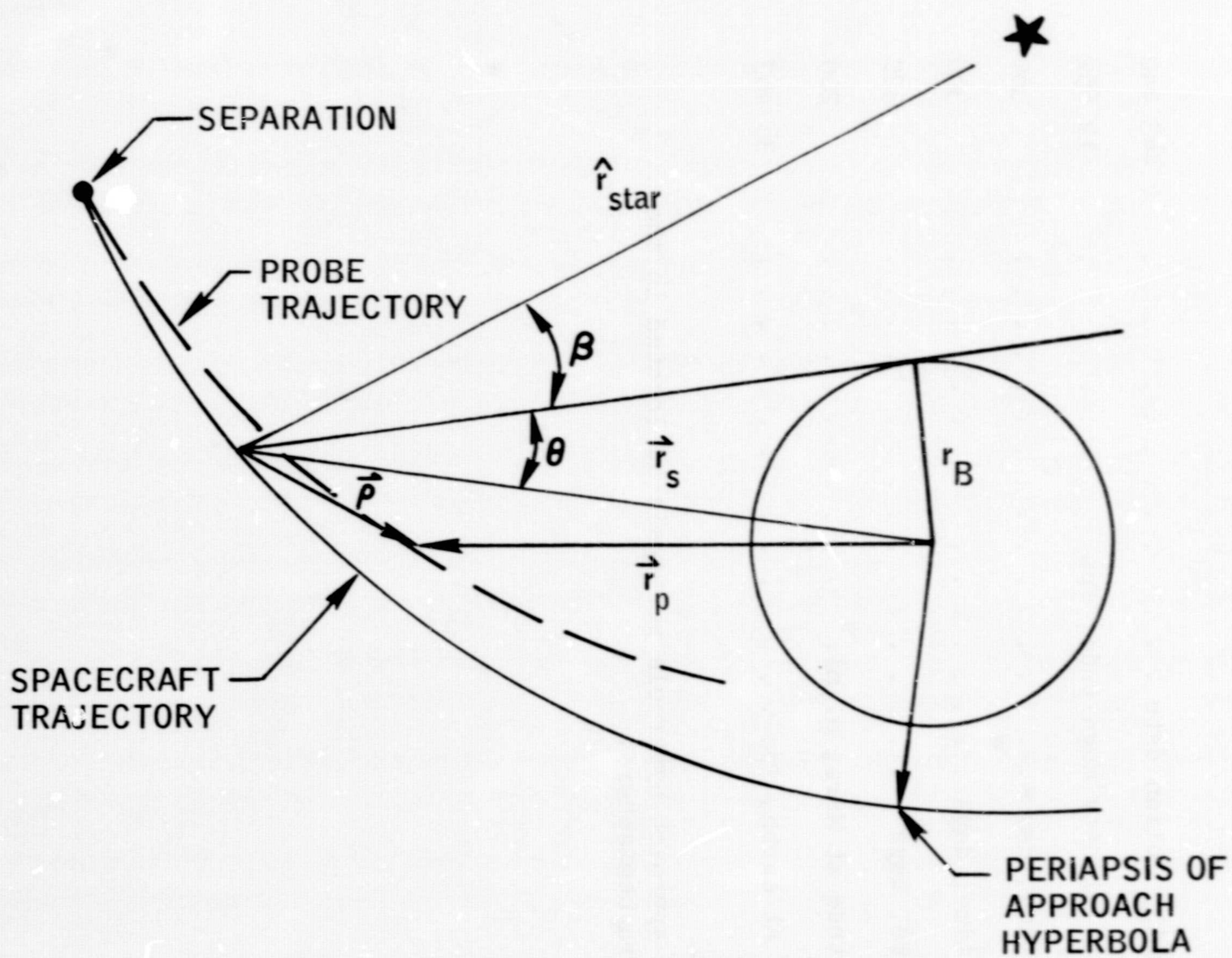


Figure 1.- Spacecraft/probe tracking geometry.

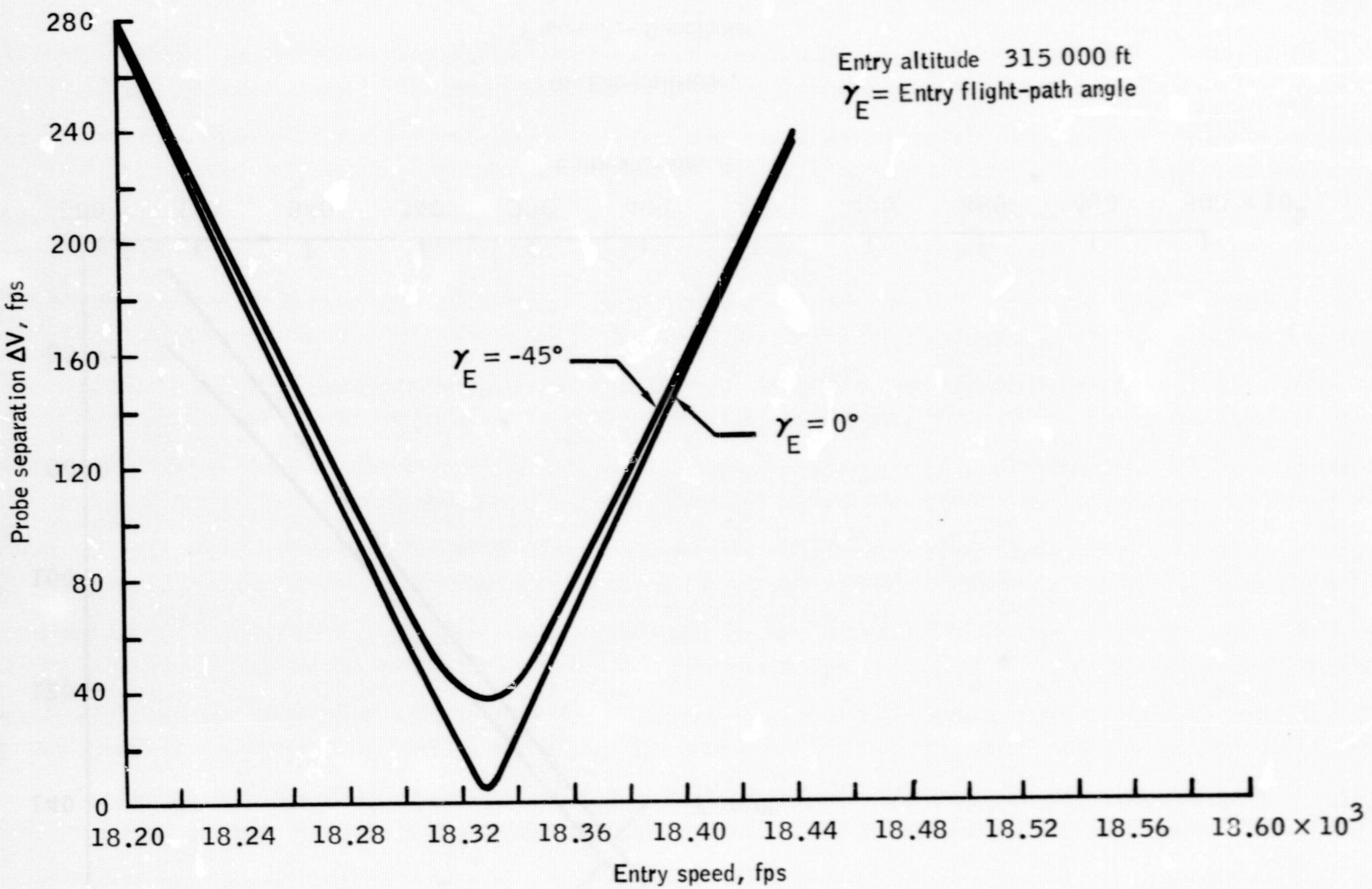


(a) Entry speed.

Figure 2.- Probe separation $\Delta V$ as a function of entry parameters.

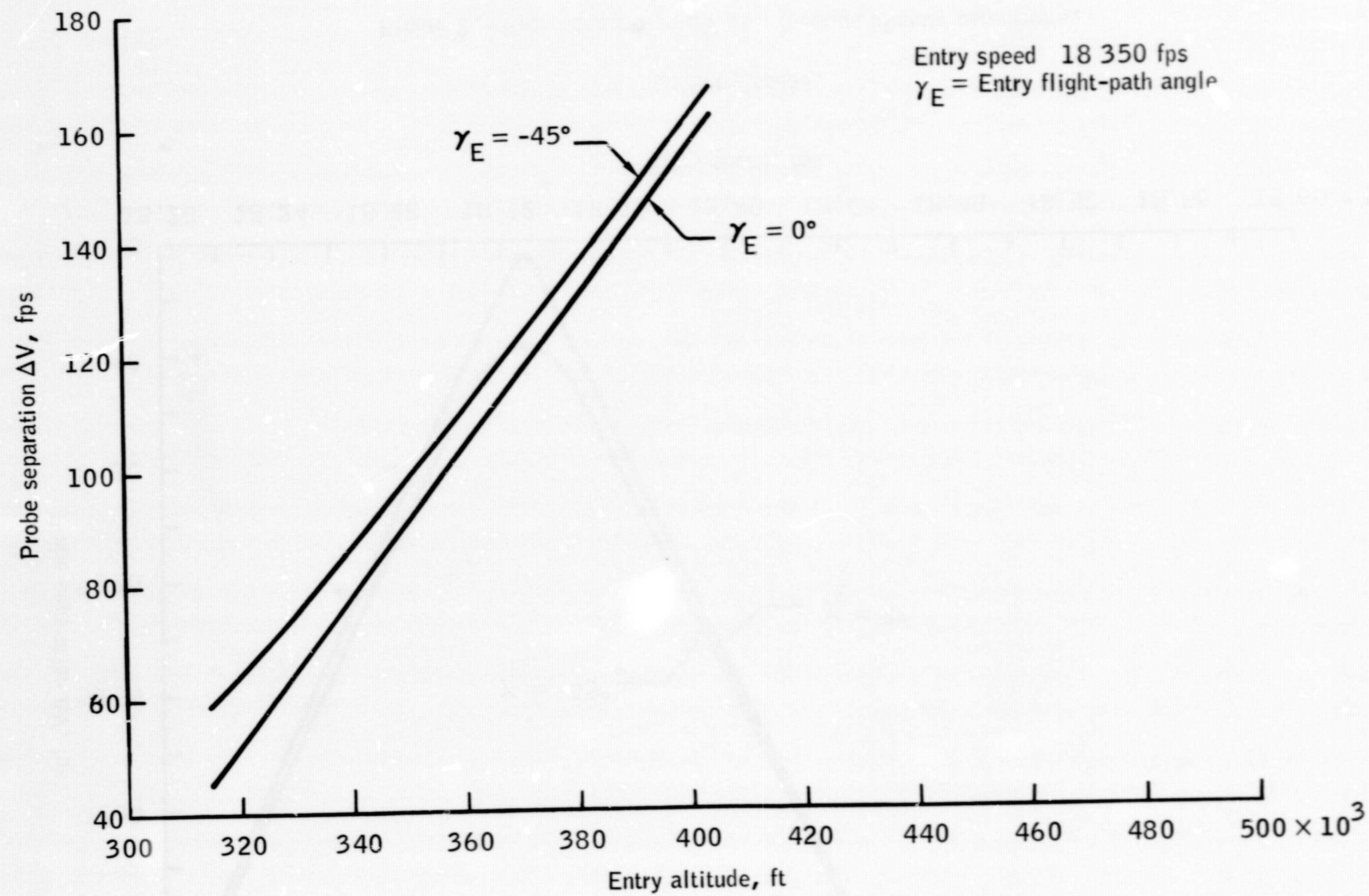


(b) Entry altitude.

Figure 2.- Concluded.

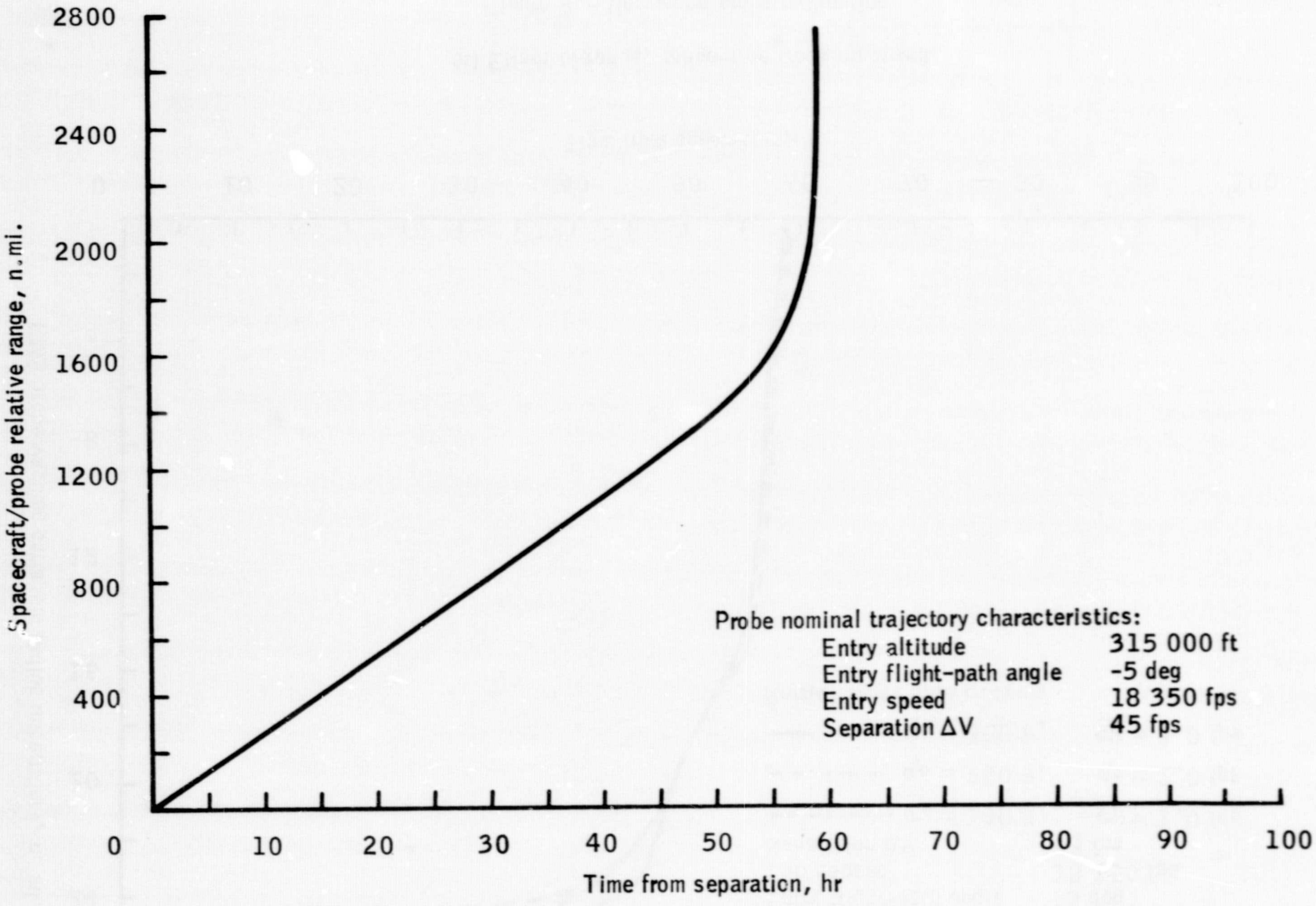


Figure 3.- Spacecraft/probe relative range as a function of time from separation.

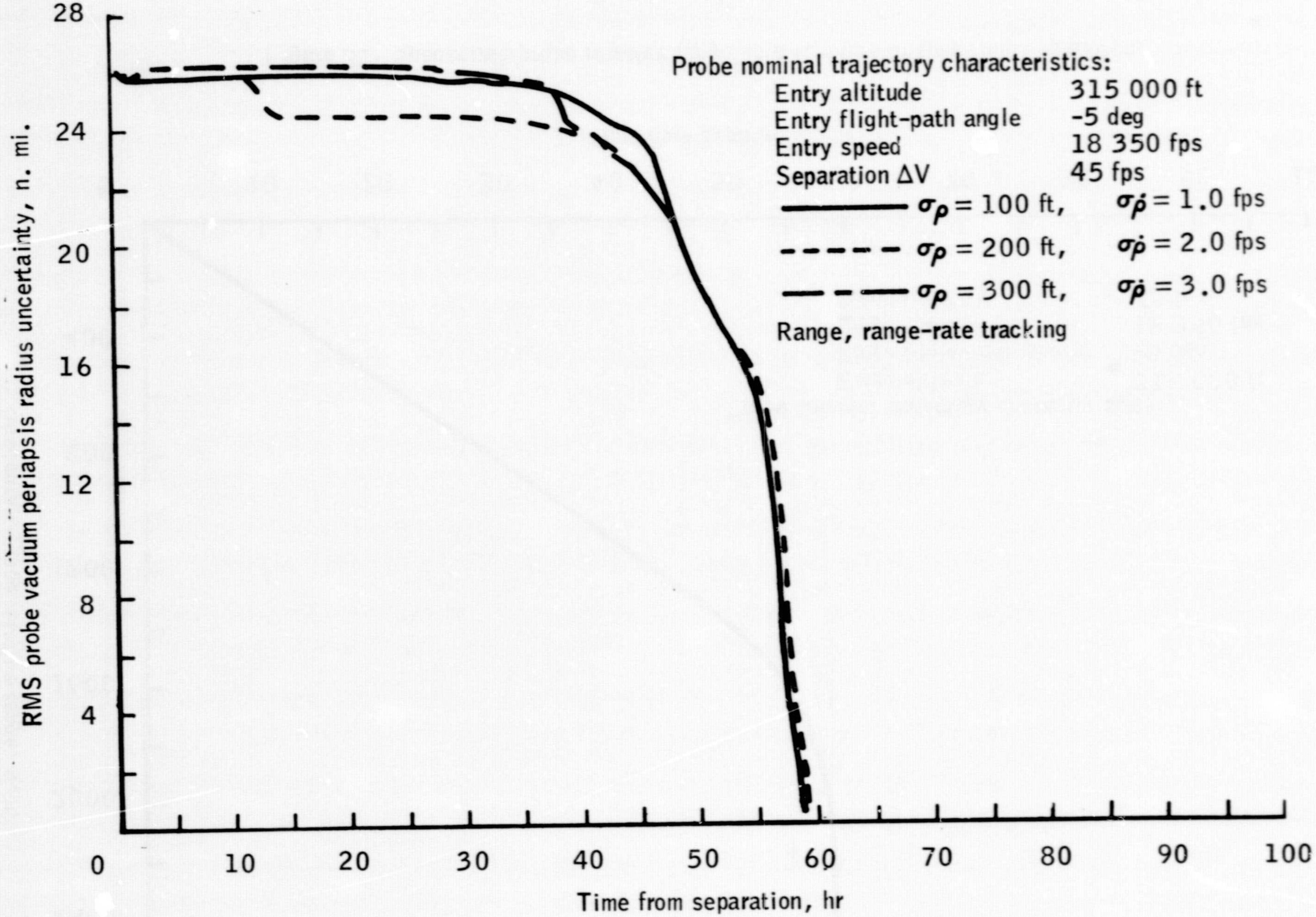


(a) Effect of range, range-rate tracking errors.

Figure 4.- Unmanned probe navigation.

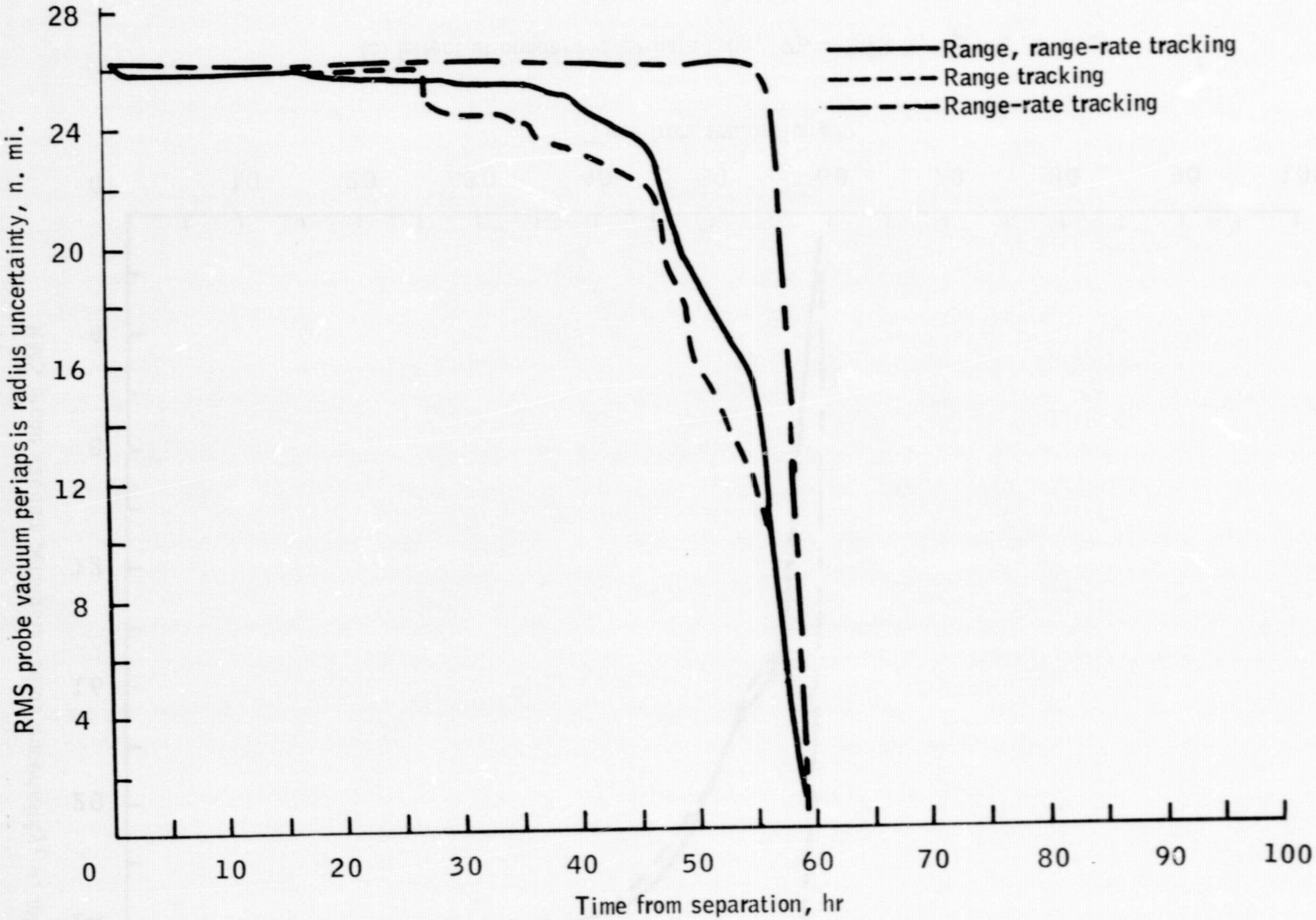


(b) Effect of onboard radar data type, $\sigma_{\rho} = 100$ ft, $\sigma_{\dot{\rho}} = 1.0$ fps.

Figure 4.- Continued.

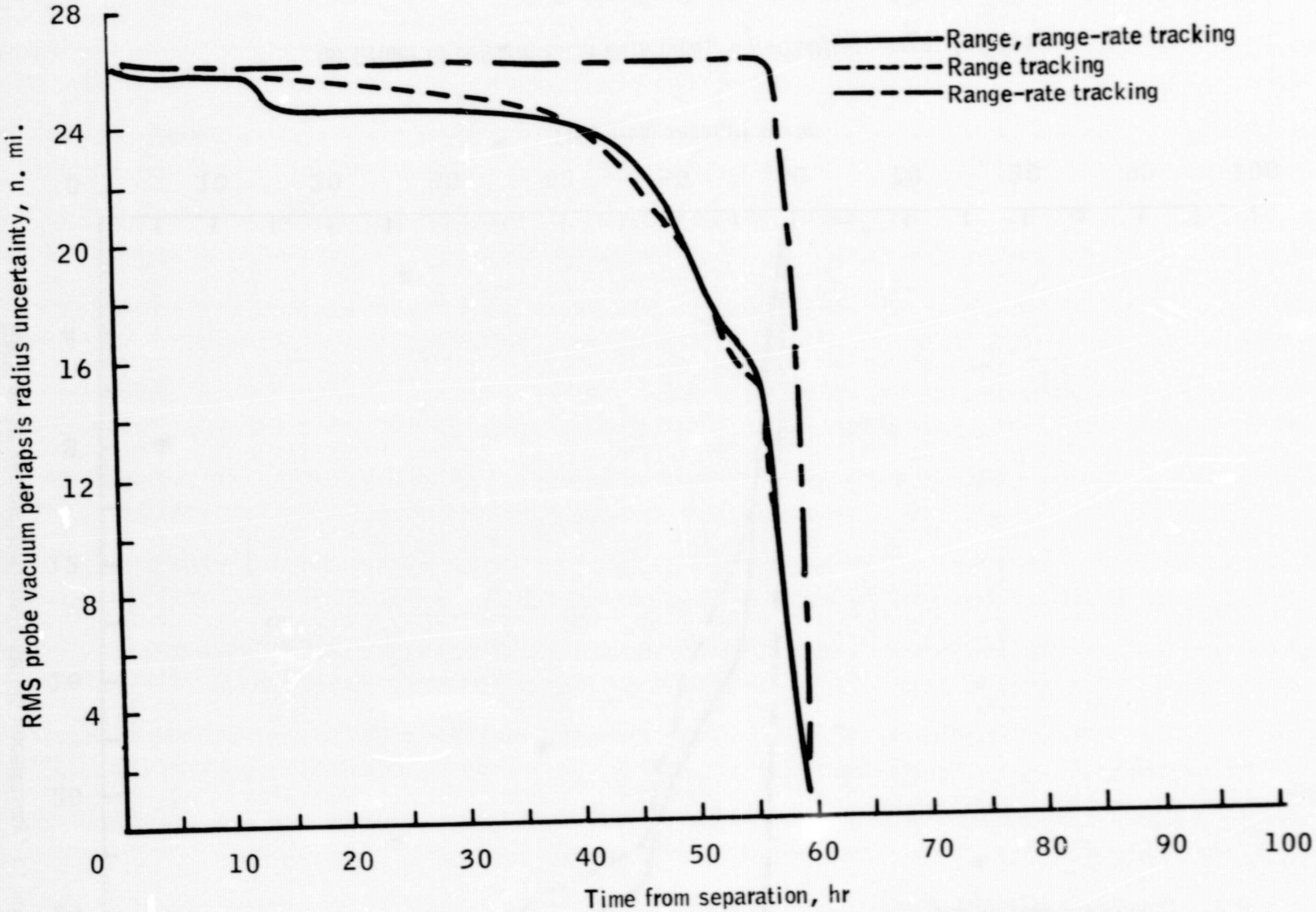


(c) Effect of onboard radar data type, $\sigma_{\rho} = 200$ ft, $\sigma_{\dot{\rho}} = 2.0$ fps.

Figure 4.- Continued.

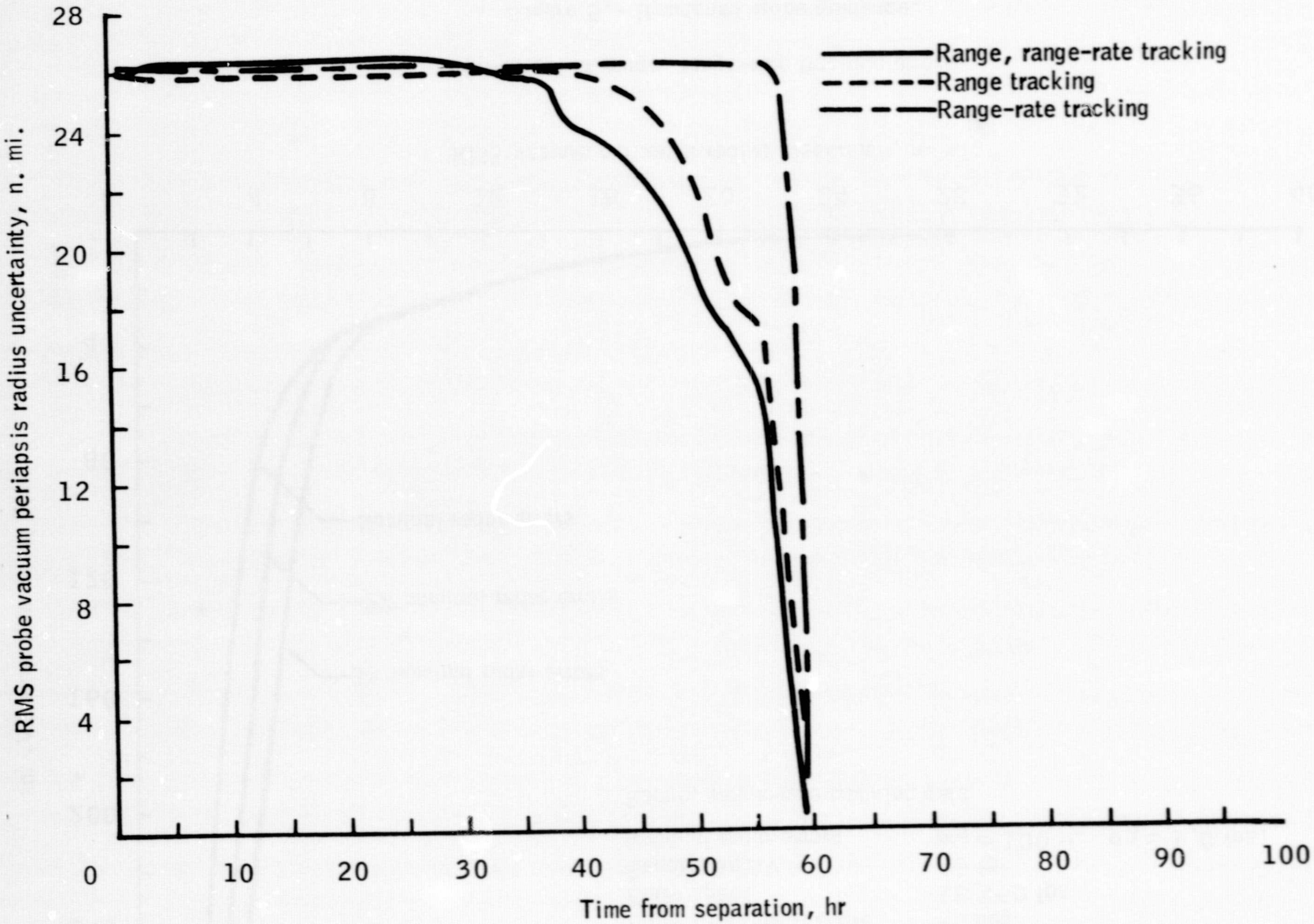


(d) Effect of onboard radar data type, $\sigma_\rho = 300$ ft, $\sigma_{\dot\rho} = 3.0$ fps.

Figure 4.- Concluded.

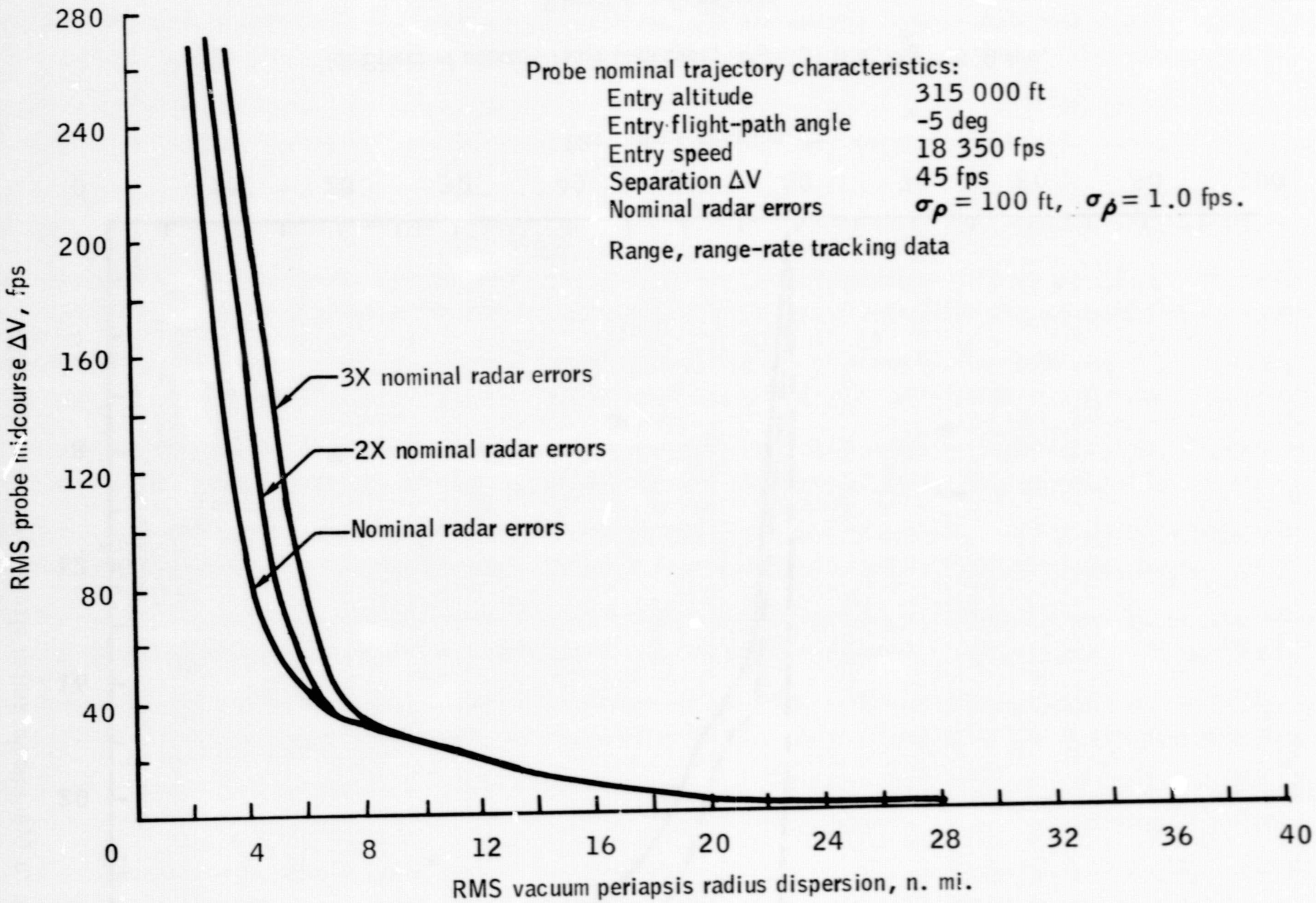


(a) Effect of range, range-rate tracking errors.

Figure 5.- Unmanned probe guidance.

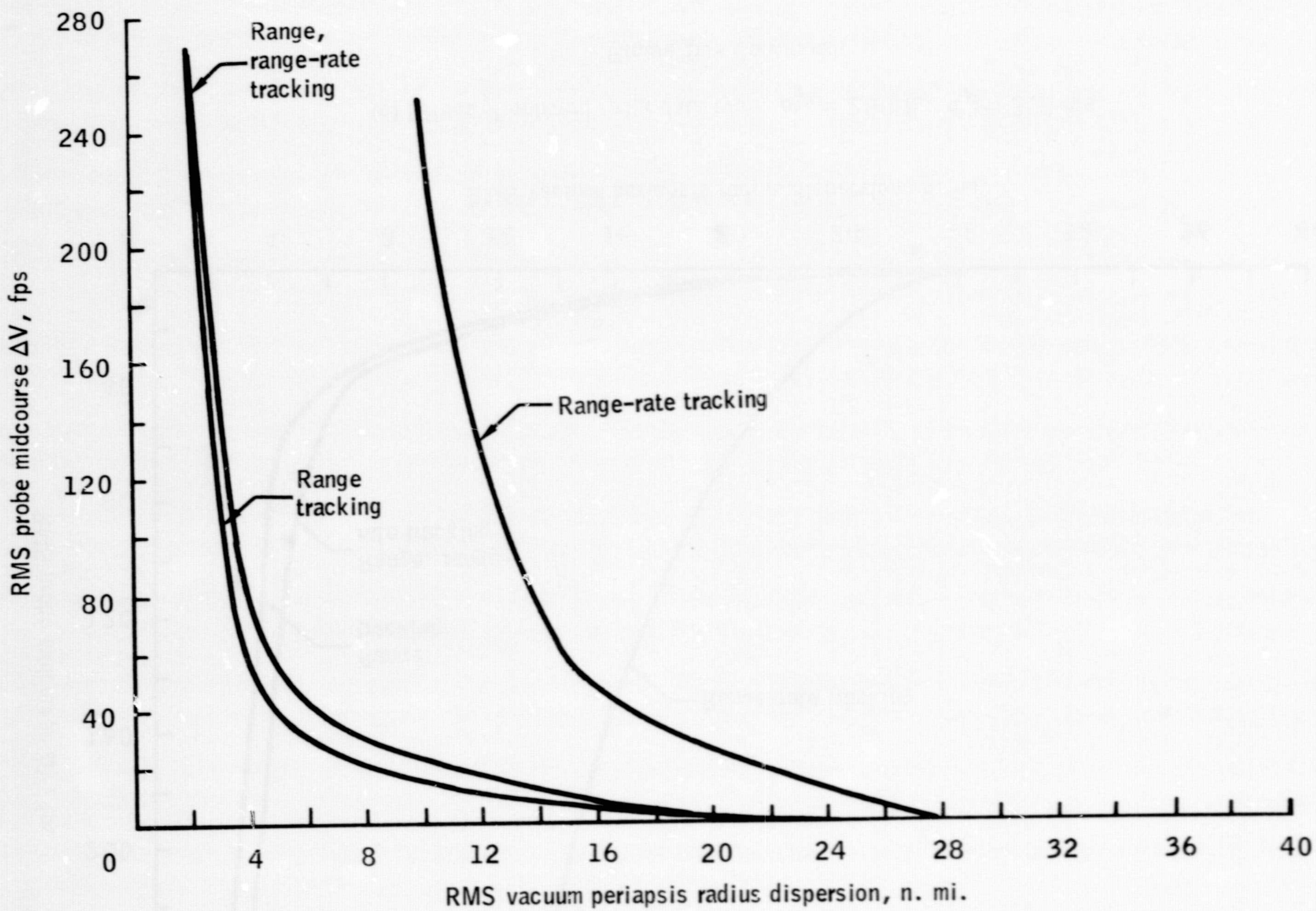


(b) Effect of onboard radar data type, $\sigma_\rho = 100$ ft, $\sigma_{\dot{\rho}} = 1.0$ fps.

Figure 5.- Continued.

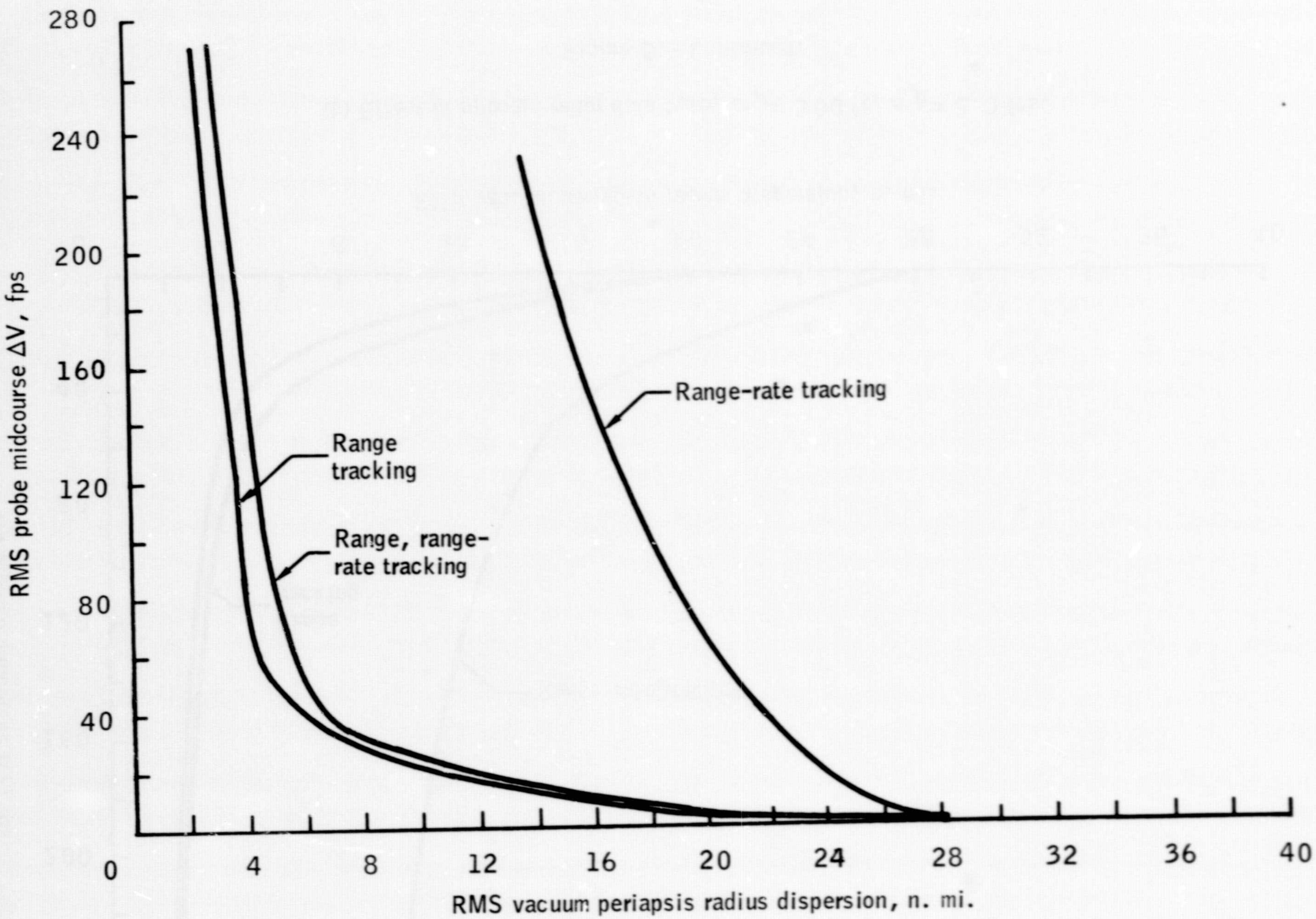


(c) Effect of onboard radar data type, $\sigma_{\rho} = 200$ ft, $\sigma_{\dot{\rho}} = 2.0$ fps.

Figure 5.- Continued.

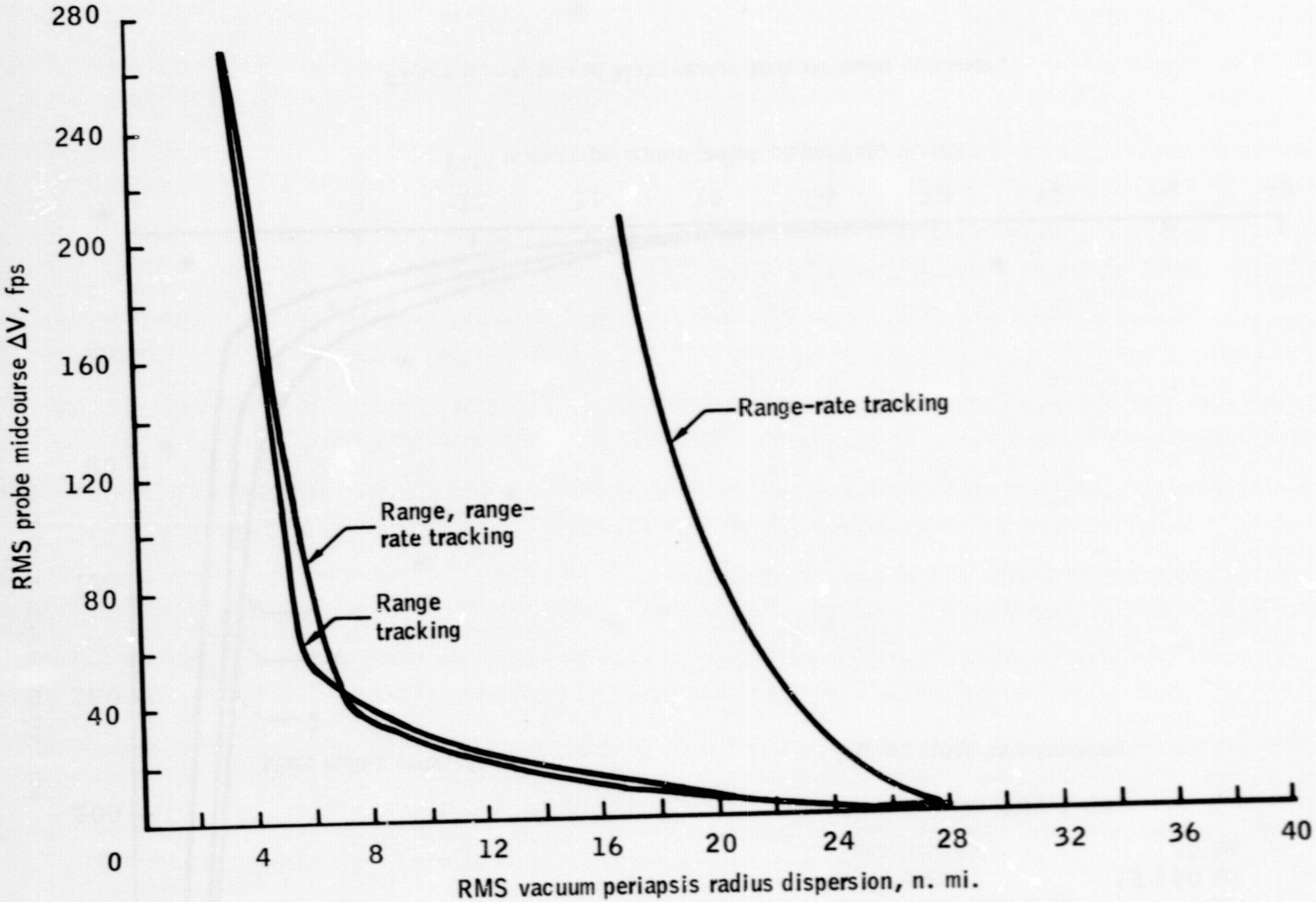


(d) Effect of onboard radar data type, $\sigma_\rho = 300$ ft, $\sigma_{\dot{\rho}} = 3.0$ fps.

Figure 5.- Concluded.

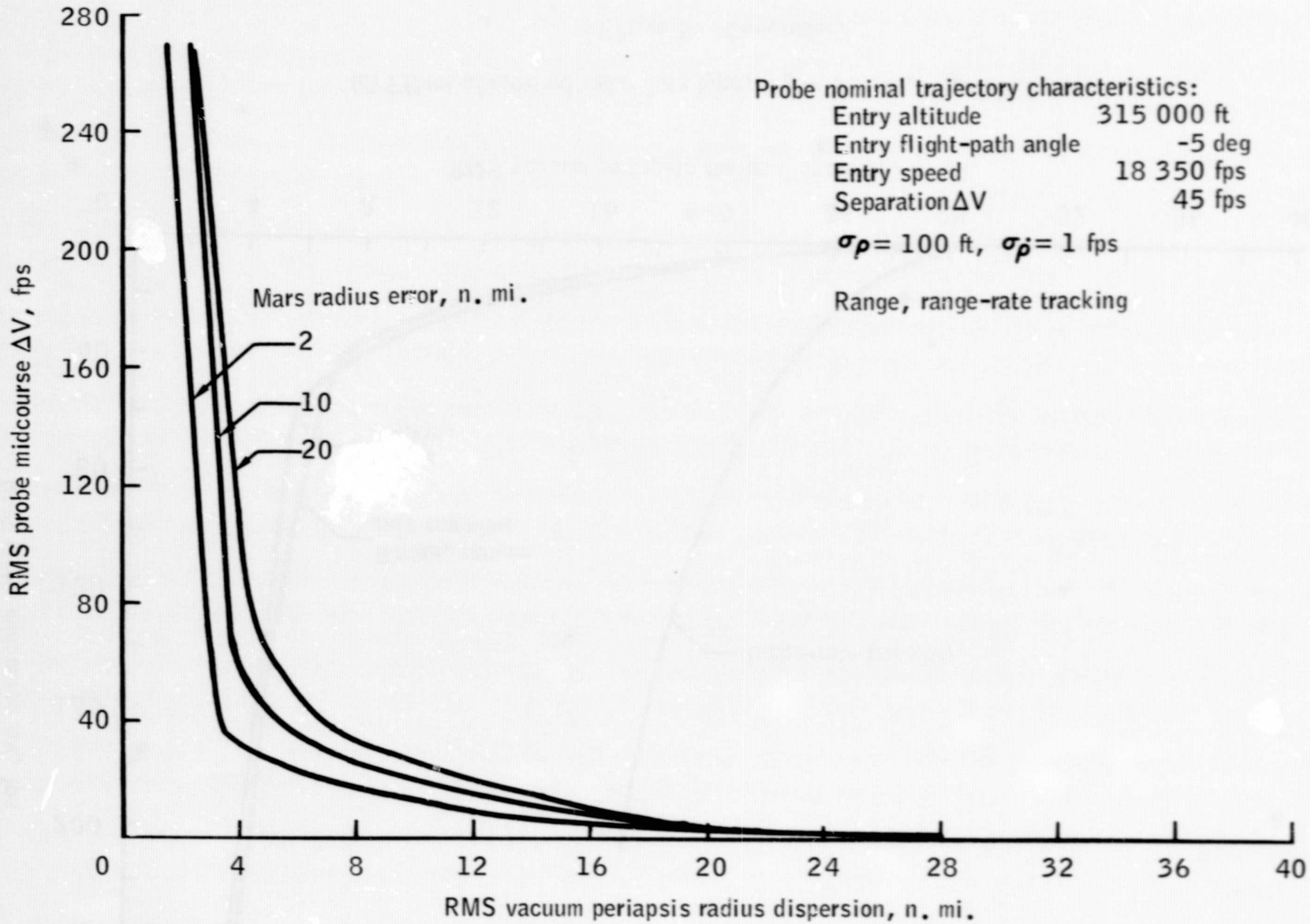


Figure 6.- Effect of Mars radius error on probe guidance.

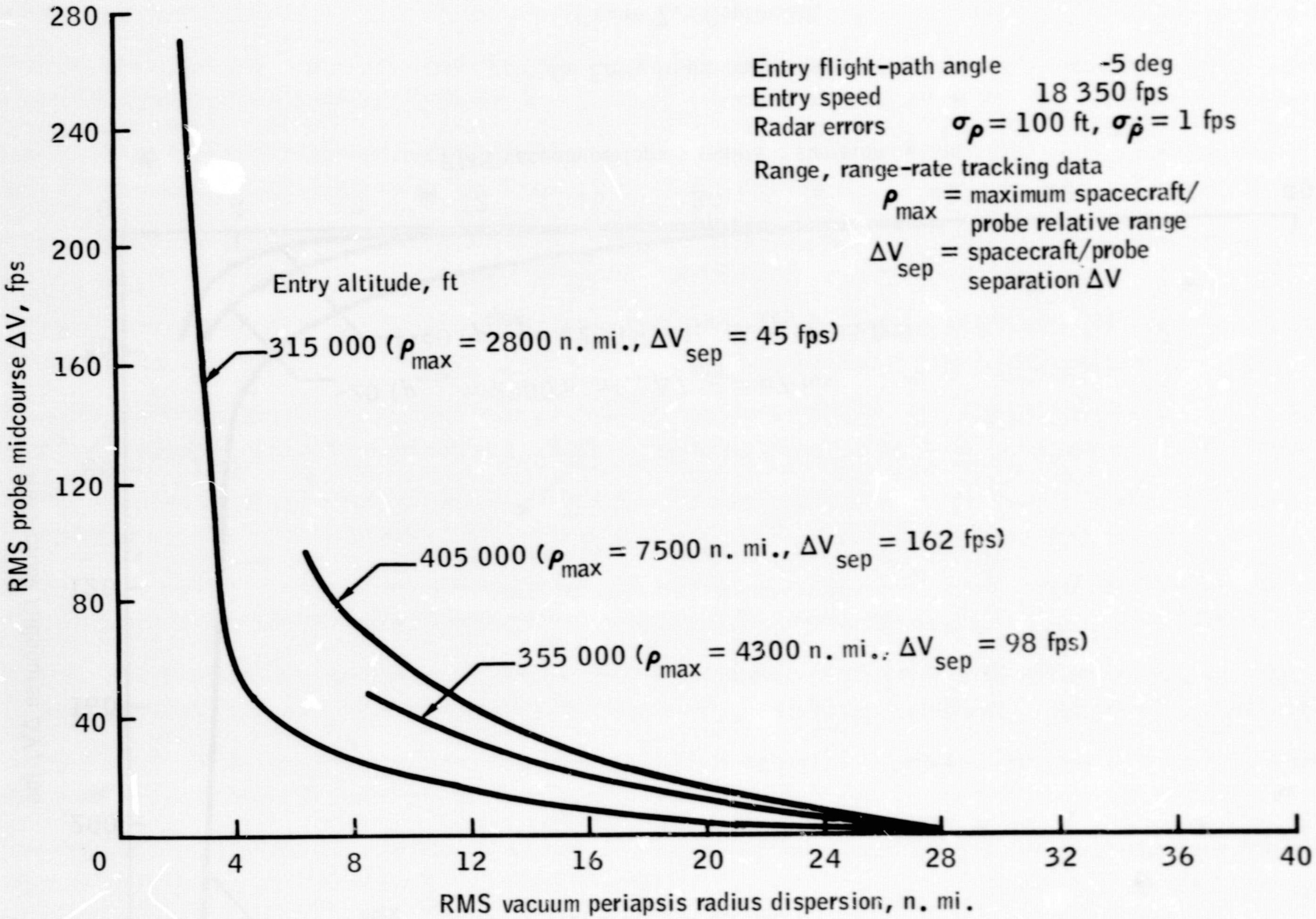


(a) Entry altitude.

Figure 7.- Influence of nominal trajectory parameter variation on probe guidance.

31

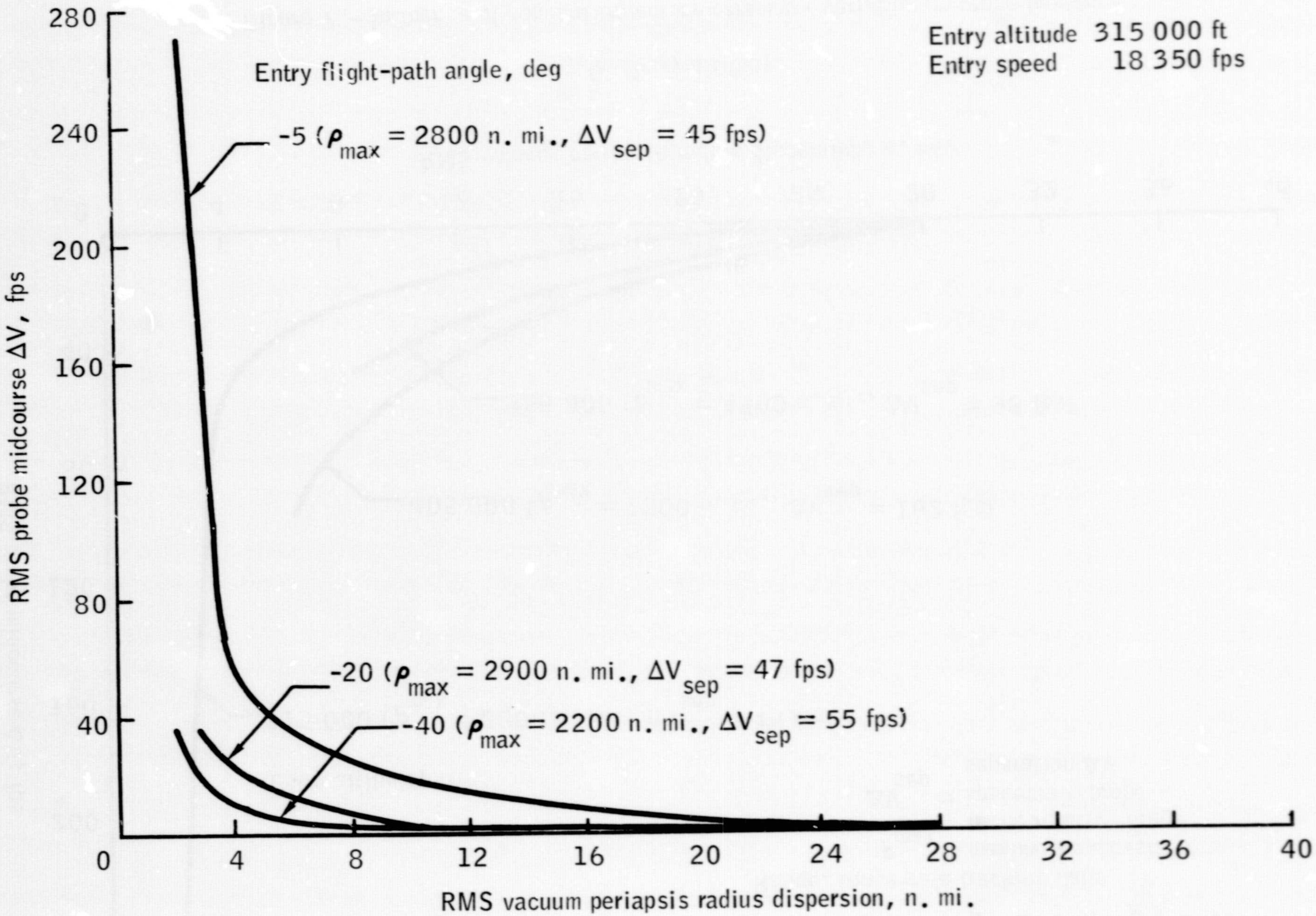


(b) Entry flight-path angle.

Figure 7.- Continued.

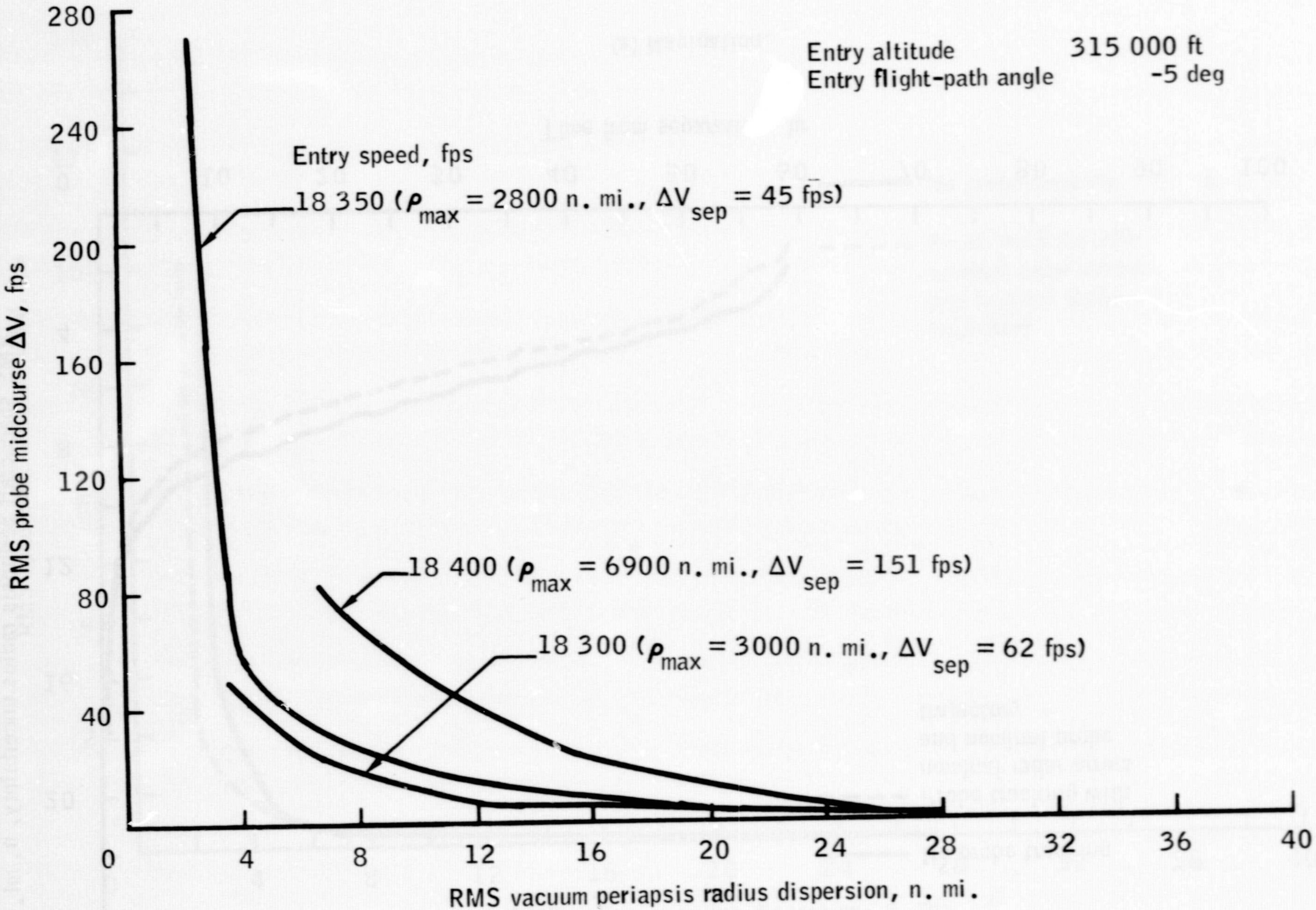


(c) Entry speed.

Figure 7.- Concluded.

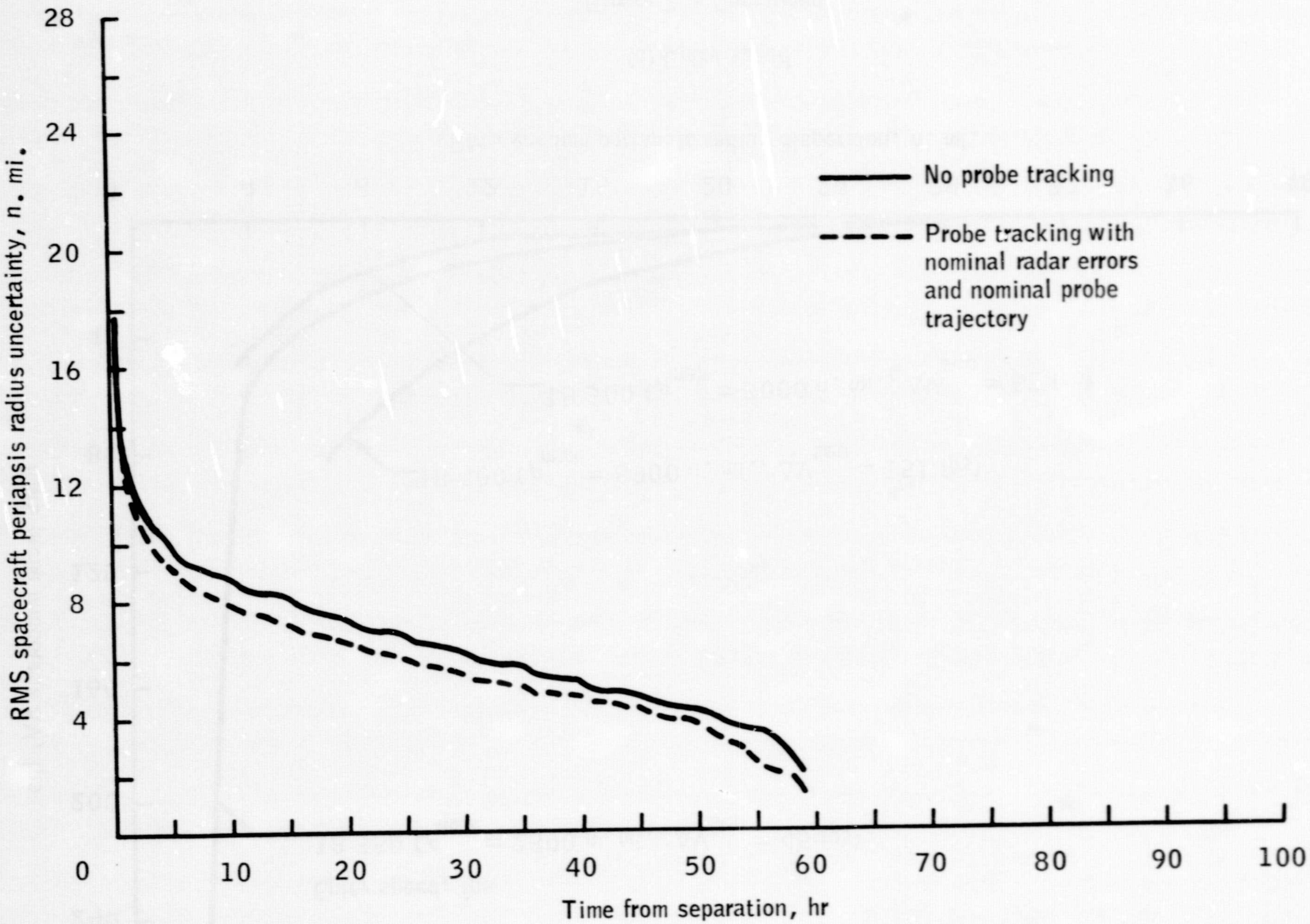


(a) Navigation.

Figure 8.- Spacecraft errors.

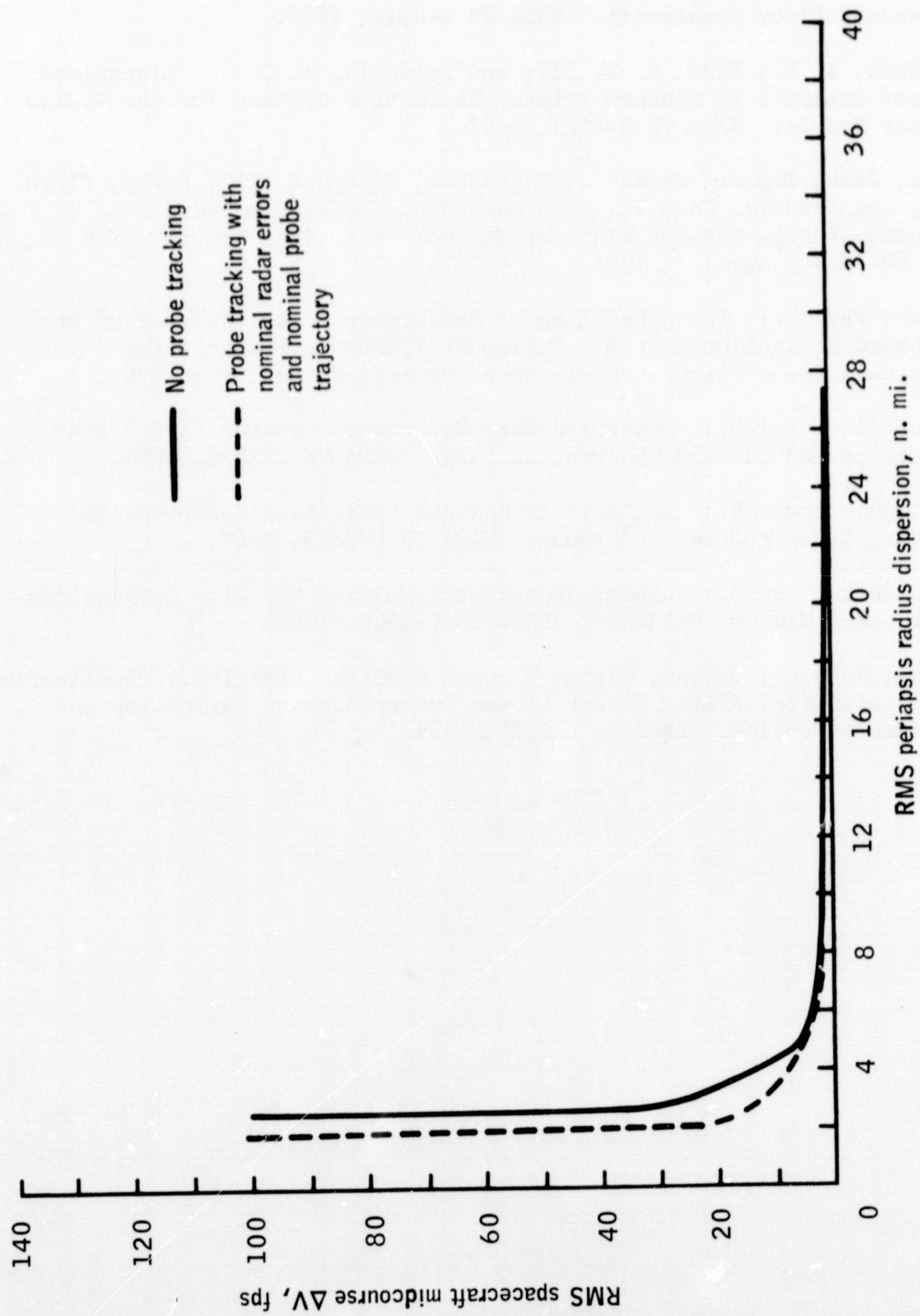


(b) Guidance.

Figure 8.- Concluded.

REFERENCES

1. Murtagh, Thomas B.; Lowes, Flora B.; and Bond, Victor R.: Navigation and Guidance Analysis of a Mars Probe Launched From a Manned Flyby Spacecraft. NASA TN D-4512, 1968.

2. Suddath, J. H.; Kidd, R. H. III; and Reinhold, A. G.: A Linearized Error Analysis of Onboard Primary Navigation Systems for the Apollo Lunar Module. NASA TN D-4027, 1967.

3. Funk, Jack; Taylor, James J.; Thibodeau, Joseph R. III; Lowes, Flora B.; and McNeely, John T.: The Manned Exploration of Mars: A Minimum-Energy Mission Plan for Maximum Scientific Return. MSC IN 68-FM-70, April 1, 1968.

4. Rohde, Paul J.: The Scheduling of Measurements for Analysis of an Onboard Navigation System. Philco WDL-TR2600. Prepared for Marshall Space Flight Center under Contract NAS 8-11198, 1965.

5. Cicolani, Luigi S.: Interplanetary Midcourse Guidance Using Radar Tracking and Onboard Observation Data. NASA TN D-3623, 1966.

6. Murtagh, Thomas B.: Analysis of Sextant Navigation Measurements During Lunar Module Rendezvous. NASA TN D-3873, 1967.

7. Cicolani, Luigi S.: Linear Theory of Impulsive Velocity Corrections for Space Mission Guidance. NASA TN D-3365, 1966.

8. White, John S.; Callas, George P.; and Cicolani, Luigi S.: Application of Statistical Filter Theory to the Interplanetary Navigation and Guidance Problem. NASA TN D-2697, 1965.